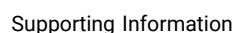


Jincheng Si, Hai-Lun Xia, Kang Zhou, Jingbai Li, Kai Xing, Jiafeng Miao, Jian Zhang, Hao Wang, Lu-Lu Qu,<sup>\*</sup> Xiao-Yuan Liu,<sup>\*</sup> and Jing Li<sup>\*</sup>

**Cite This:** *J. Am. Chem. Soc.* 2022, 144, 22170–22177



Metrics & More



*i*: Olympic Rings inspired structure;  
*ii*: excited-state intramolecular proton transfer;  
*iii*: sensitive and selective  $\text{Cr}_2\text{O}_7^{2-}$  detection

- i*: Olympic Rings inspired structure;
- ii*: excited-state intramolecular proton transfer;
- iii*: sensitive and selective  $\text{Cr}_2\text{O}_7^{2-}$  detection

Olympic rings represent one of the most inspiring symbols, which has received great interests in structural chemistry. Olympic rings-inspired molecular structures have been reported, such as those of supramolecular species synthesized by self-assembly processes.<sup>33–35</sup> It would be wonderful if we

**Published:** November 23, 2022



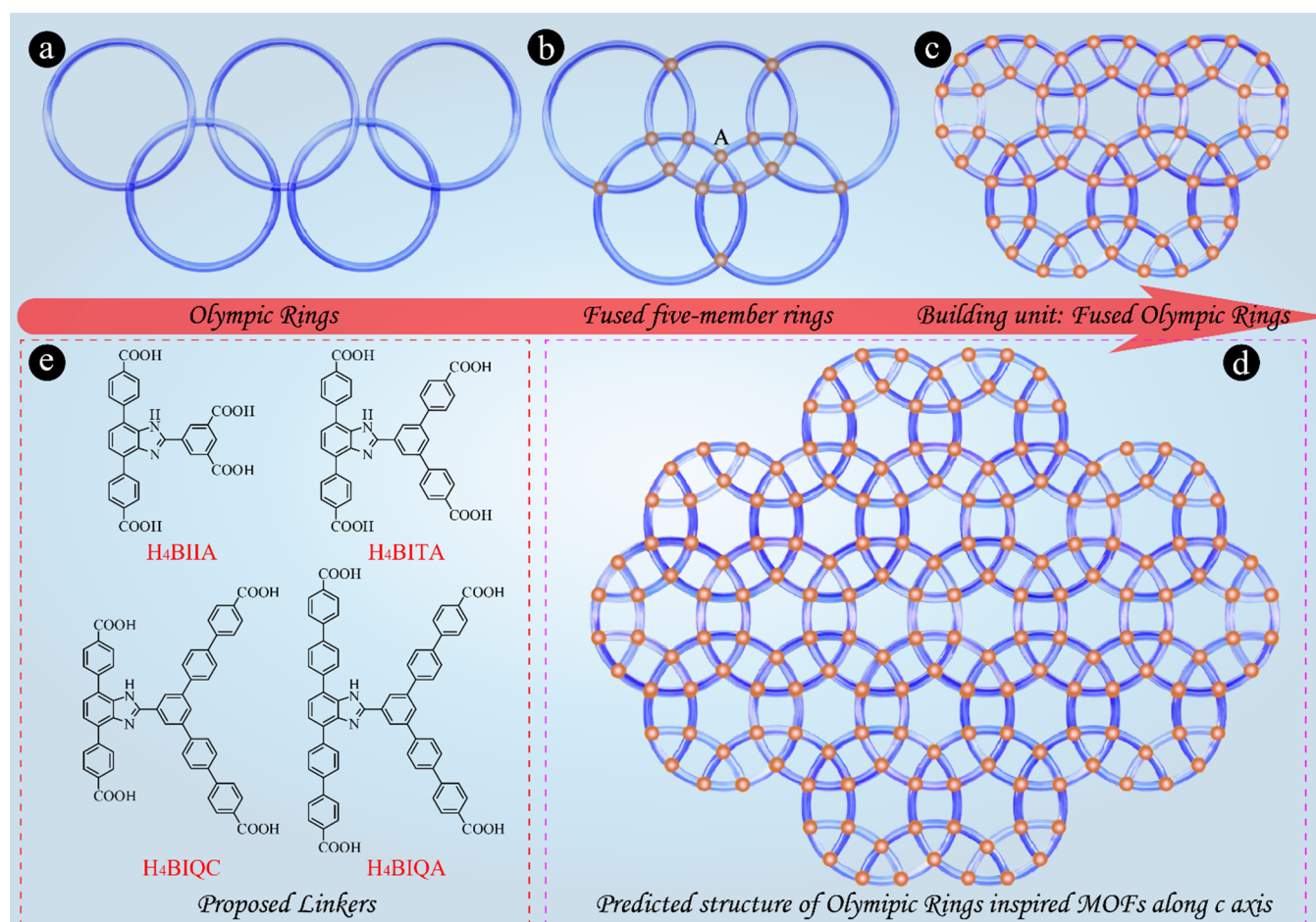


**Figure 1.** Schematic diagram illustrating the design of the Olympic rings-inspired MOFs. (a) Olympic rings, (b) fused five-member rings derived from Olympic rings, (c) building unit: fused Olympic rings, (d) extended 2D layer structure as the predicted structure of Olympic rings-inspired MOFs viewed along the *c*-axis, and (e) proposed linkers to prepare the Olympic rings-inspired MOFs.

channels coexist. Based on the crystal structure analysis of NU-1000 (Figures S1 and S2) and similar MOFs, we envision that the Olympic rings-inspired MOFs might also be formed using tetratopic carboxylates and Zr<sub>6</sub> clusters.

The 2D model depicted in Figure 1d can be considered as the predicted structure of Olympic rings-inspired MOF and can be extended along the *c*-axis to generate the overall 3D framework, which is similar to what is observed in *csq*-type MOFs. With the potential structure in mind, another challenge is to design organic linkers that can be utilized to construct the MOFs with the designed underlying net. To form the structure having the same shape as the Olympic rings will require the linkers with some extent of bendability to build the circle. Examples are rare in reported MOFs. In this study, we proposed four linkers with potentially suitable bendability (Figure 1e).

In the present work, the use of reticular chemistry as described above enabled us to construct a unique MOF, HIAM-4017 (HIAM = Hoffmann Institute of Advanced Materials; 40 = zirconium), with an unprecedented (4,8)-*c* underlying net topology termed *jcs* inspired from Olympic rings. HIAM-4017 was obtained by the judicious design and synthesis of a nonsymmetric organic linker and its incorporation into the Zr-based framework. HIAM-4017 shows high porosity and excellent chemical and thermal stability. Furthermore, excited-state intramolecular proton transfer

(ESIPT) was induced in an isorecticular MOF, HIAM-4018, with a large Stokes shift of 155 nm via the addition of a hydroxyl group onto the linker skeleton to generate strong OH...N interactions. Such interactions were analyzed thoroughly by employing density functional theory (DFT). Because of its good thermal and chemical stability and strong blue emission, nanosized HIAM-4017 and HIAM-4018 were fabricated and used for Cr<sub>2</sub>O<sub>7</sub><sup>2-</sup> detection with high sensitivity and selectivity.

## RESULTS AND DISCUSSION

**Olympic Rings-Inspired MOFs.** Bearing aforementioned consideration in mind, we carried out a literature search and found that the [1,1':4',1''-terphenyl]-4,4''-dicarboxylic acid moiety in some linkers can be bent in the resultant MOF structures, such as BUT-39 (Figure S3).<sup>39</sup> Therefore, we designed and synthesized four nonsymmetric tetratopic carboxylate linkers with a “K-shaped” structure but different molecular length via Suzuki–Miyaura coupling followed by the saponification reaction (detail procedures in the Supporting Information), namely, 5-(4,7-bis(4-carboxyphenyl)-1H-benzo-[*d*]imidazol-2-yl)isophthalic acid (H<sub>4</sub>BIIA), 5'-(4,7-bis(4-carboxyphenyl)-1H-benzo[*d*]imidazol-2-yl)-[1,1':3',1''-terphenyl]-4,4''-dicarboxylic acid (H<sub>4</sub>BITA), 5''-(4,7-bis(4-carboxyphenyl)-1H-benzo[*d*]imidazol-2-yl)-[1,1':4',1'':3'',1'''-quinquephenyl]-4,4'''-dicarboxylic

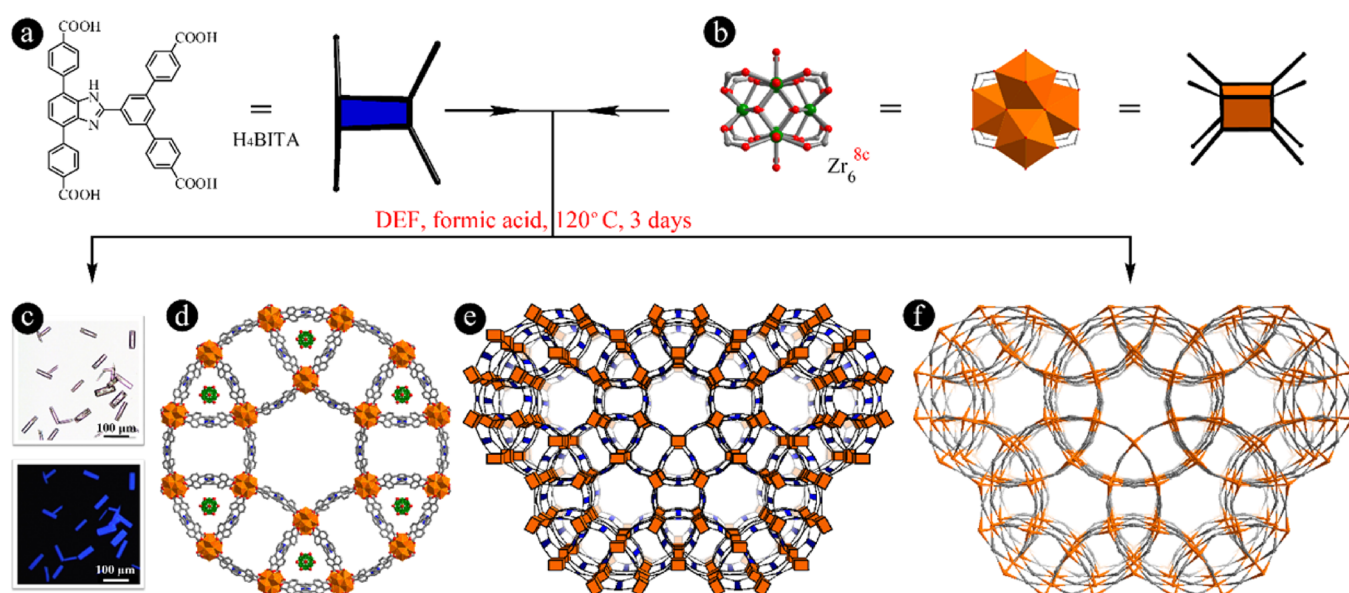


**Figure 2.** (a) Molecular structure of 4-connected  $H_4BITA$  in HIAM-4017; (b) 8-connected  $Zr_6$  cluster in HIAM-4017; (c) bright-field (above) and photoluminescence (below) single-crystal images of HIAM-4017 under 365 nm excitation; (d) single-crystal structure and (e and f) the *jcs* net topology of HIAM-4017 (Color scheme: gray, C; green, Zr; red, O; blue, N).

acid ( $H_4BIQC$ ), and 5''-(4,7-bis(4'-carboxy-[1,1'-biphenyl]-4-yl)-1H-benzo[*d*]imidazol-2-yl)-[1,1':4',1'':3'',1''':4''',1''''-quinquephenyl]-4,4'''-dicarboxylic acid ( $H_4BIQA$ ), as depicted in Figure 1e, which were then used to prepare Olympic rings-inspired Zr-MOFs.

A typical synthesis of HIAM-4017 is schematically shown in Figure 2a,b: a 5 mL vial containing 3 mL of *N,N*-diethylformamide, 23.3 mg of  $ZrCl_4$ , 10 mg of  $H_4BITA$ , and 0.5 mL of formic acid was placed in a preheated oven at 120 °C for 3 days.

Colorless single crystals were obtained with bright blue emission under 365 nm excitation (Figure 2c). Single-crystal X-ray diffraction (sc-XRD) analysis revealed that HIAM-4017 crystallizes in the hexagonal crystal system with the  $P6/mmm$  space group (Table S1). As shown in Figures 2d and S4, in the structure of HIAM-4017, each  $Zr_6$  cluster is coordinated to eight fully deprotonated BITA linkers and eight terminal  $H_2O/OH^-$  groups. Each deprotonated tetratopic linker BITA is connected to four  $Zr_6$  clusters. These combinations give the overall formula of HIAM-4017 as  $Zr_6O_4(OH)_8(H_2O)_4(BITA)_2$ . One expected feature in HIAM-4017 is that a circular unit, namely, a single ring, is formed via the combination of 12 linkers and 12 8-c  $Zr_6$  clusters (Figure 2d), which can be ascribed to the bendability of  $H_4BITA$  when confined in the MOF matrix (Figure S5). Further analysis demonstrates that HIAM-4017 possesses a totally different structure compared with all reported tetratopic linker-based Zr-MOFs.<sup>40</sup> Rather, it is a 3-nodal (4,4,8)-c net with the point symbol of  $\{4^{16}.6^{12}\}\{4^4.6^2\}_2$  and represents an unprecedented topology for MOFs. The net is denoted as *jcs* (Figures 2e,f and S6). Three types of one-dimensional open channels are formed along the *c*-axis, that is, one triangular channel, one quadrilateral channel, and one hexagonal channel (Figures 2e and S4). Another most interesting structural feature in HIAM-4017 is that there are isolated  $Zr_6$  clusters confined in the triangle channels with 42.4% occupation, which has been rarely reported for Zr-MOFs. However, the other three linkers,  $H_4BIIA$ ,  $H_4BIQC$ , and  $H_4BIQA$  did not lead to

isorecticular MOFs in spite of many attempts using different solvents (i.e., *N,N*-diethylformamide, *N,N*-dimethylformamide, and *N,N*-dimethylacetamide) and acid modulators (i.e., formic acid, acetate acid, benzoic acid, trifluoroacetic acid, 2-fluorobenzoic acid, and propionic acid). In the case of  $H_4BIQA$ , which was synthesized by incorporating an additional phenyl ring in each arm of  $H_4BITA$ , the reaction hardly took place because of its extremely poor solubility in all solvents. These results reveal that this unique MOF topology has stringent requirements on the linker geometry (e.g., shape, size, and relative lengths of the two dicarboxylate moieties).

The phase purity of HIAM-4017 bulk samples was confirmed by the comparison of the experimental powder X-ray diffraction (PXRD) pattern of as-synthesized HIAM-4017 with the simulated one (Figure 3a). The permanent porosity of HIAM-4017 was examined by  $N_2$  sorption experiments at 77 K. As depicted in Figure 3b, HIAM-4017 shows type IV isotherms, indicative of the hierarchically porous structure with both micropores and mesopores. The Brunauer–Emmett–Teller (BET) surface area for HIAM-4017 is 1083 m<sup>2</sup>/g calculated from the nitrogen sorption data. The experimental total pore volume is 0.536 cm<sup>3</sup>/g for HIAM-4017. According to the  $N_2$  sorption data, the pore size distribution analysis based on the DFT method confirmed the hierarchical porous structure with micropores at 12.3 and 17.7 Å and mesopores at 26.5 Å for HIAM-4017 (Figure S7).

Thermal and chemical stability of HIAM-4017 under different conditions was evaluated to ensure its suitability for potential real-world applications. As observed from the PXRD pattern, the framework maintained its structural integrity after thermal activation under a dynamic vacuum at 120 °C for 12 h, indicating the rigid structural nature of HIAM-4017. The temperature-dependent in situ PXRD and thermogravimetric analysis (TGA) also indicated that HIAM-4017 remains crystalline up to 500 °C (Figures S8 and S9). Chemical stability of HIAM-4017 was tested under various conditions, including soaking in water at room temperature, in boiling water, and in 0.1 mM NaOH, 2 M HCl, and concentrated HCl



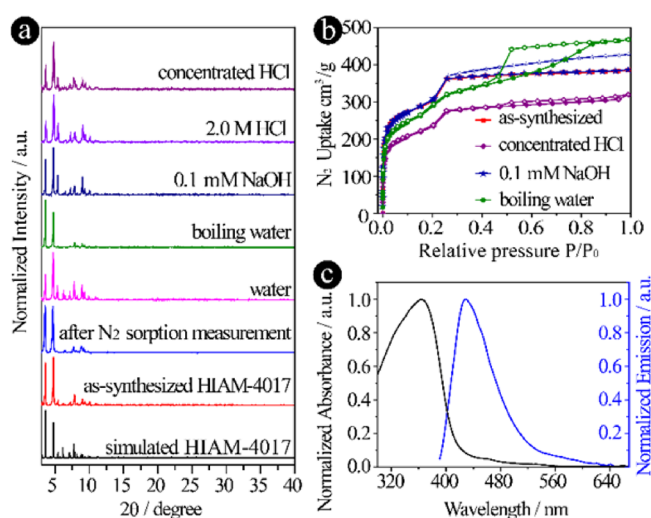


**Figure 3.** (a) PXRD patterns of the simulated, as-synthesized HIAM-4017, after N<sub>2</sub> sorption measurement and treatment under different conditions for 24 h; (b) N<sub>2</sub> adsorption–desorption isotherms of HIAM-4017 at 77 K after treatment under different conditions for 24 h; (c) solid-state UV–vis absorption and emission spectra of HIAM-4017.

at room temperature for 24 h, respectively. As shown in Figure 3a, the nearly identical PXRD patterns reveal that the long-range order of HIAM-4017 was maintained very well under all the tested conditions. No significant changes were observed on the single crystals after these treatments (Figure S10). The isolated Zr<sub>6</sub> clusters remain confined in the triangular channels, confirmed by sc-XRD analysis (Figure S11). The corresponding BET surface areas and total pore volumes were estimated to be 986 m<sup>2</sup>/g and 0.681 cm<sup>3</sup>/g, 823 m<sup>2</sup>/g and 0.457 cm<sup>3</sup>/g, and 1079 m<sup>2</sup>/g and 0.617 cm<sup>3</sup>/g after treatment in boiling water, concentrated HCl, and 0.1 mM NaOH for 24 h, respectively. These values are slightly lower than that of the as-made sample, possibly due to the structural defects resulted

from the treatment under harsh conditions. The porosity analysis of HIAM-4017 after being treated in boiling water indicates changes in the crystal and pore structure. The sizes of the three pores are approximately 9.3, 19.8, and 32.0 Å (Figure S12).

Room-temperature solid-state photoluminescence (PL) and UV–vis absorption spectra of HIAM-4017 are shown in Figure 3c. The absorption and emission maxima are at 365 and 429 nm, respectively, with the corresponding photoluminescence quantum yield (PLQY) of 32.9% under 365 nm excitation. A ~5 nm blue shift and 12 nm bathochromic shift were observed after treatment in concentrated HCl and 0.1 mM NaOH, indicating that acid and base exert limited effect on the emission property (Figure S13).

**ESIPT in Olympic Rings-Inspired MOFs and Computational Study.** As has been reported, ESIPT is an interesting photochemical process with a large Stokes shift induced by the intramolecular hydrogen bond.<sup>41</sup> ESIPT is a four-level photocycle process between the enol form, the excited enol form, the excited keto form, and the keto form. The large Stokes shift results from the high energy absorption in the enol form and low energy emission from the keto form. Usually, this phenomenon happens between the OH group and N or O atoms, which has received increasing attention in MOFs for chemical sensing and other related applications in recent years.<sup>42–47</sup>

To extend the linker diversity in our study and introduce ESIPT in the resultant MOFs, a OH group was added to H<sub>4</sub>BITA to form 5'-(4,7-bis(4-carboxyphenyl)-1H-benzo[d]-imidazol-2-yl)-4'-hydroxy-[1,1':3',1''-terphenyl]-4,4''-dicarboxylic acid (H<sub>4</sub>BIHTA) (Figure 4a). The corresponding MOF, HIAM-4018, was then prepared using the similar reaction conditions as HIAM-4017. Light yellow single crystals of HIAM-4018 were obtained, which emit bright yellow light, as depicted in Figure 4b. As shown in Figure 4c, the PXRD pattern of the as-synthesized HIAM-4018 matches well with that of the simulated HIAM-4017, confirming its isoreticular

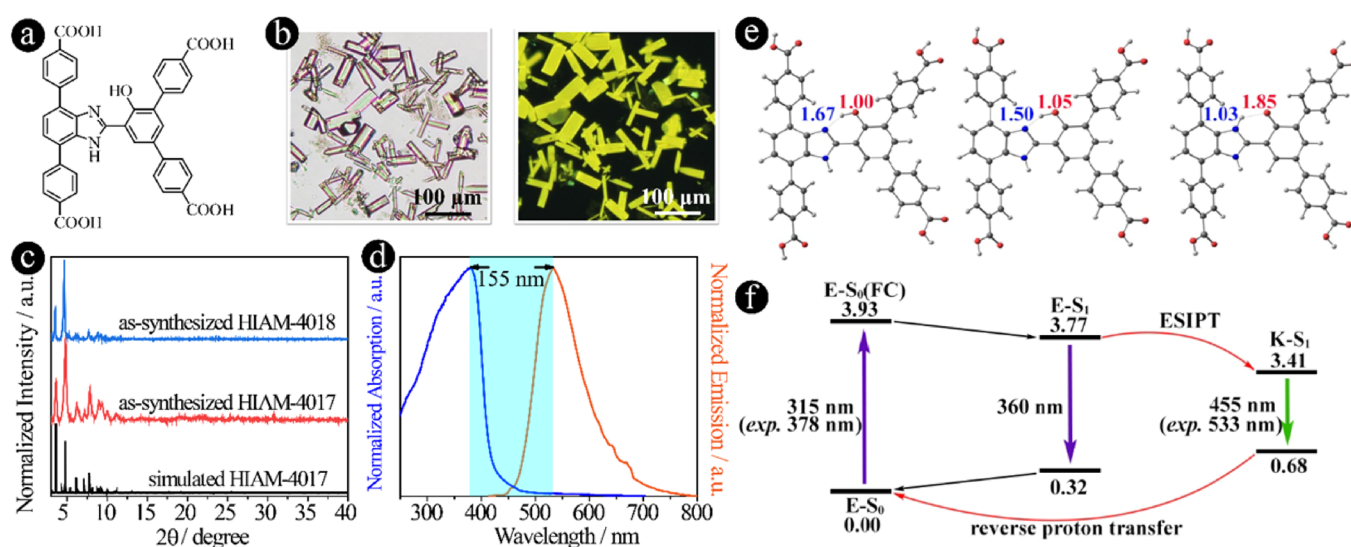


**Figure 4.** (a) Molecular structure of H<sub>4</sub>BIHTA; (b) bright-field (left) and photoluminescence (right) single-crystal images of HIAM-4018 under 365 nm excitation; (c) PXRD patterns of the simulated, as-synthesized HIAM-4017 and HIAM-4018; (d) solid-state UV–vis absorption and emission spectra of HIAM-4018; (e) equilibrium geometries of H<sub>4</sub>BIHTA at E-S<sub>0</sub>, E-S<sub>1</sub>, and K-S<sub>1</sub> states, optimized with CAM-B3LYP/cc-pVDZ and (f) corresponding energy profile computed with CAM-B3LYP/cc-pVTZ (The N–H and O–H distances are shown in blue and red texts, respectively; the distance unit is Angstrom, and the energy unit is eV).

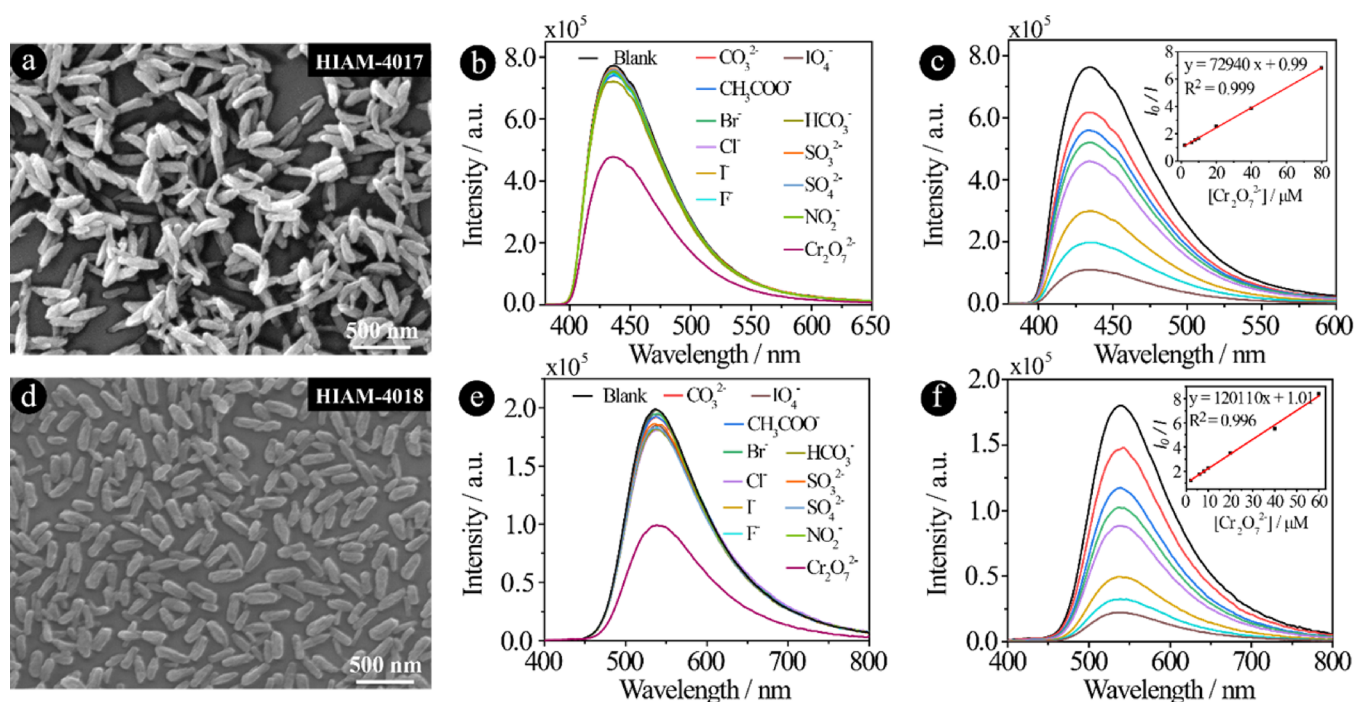


**Figure 5.** SEM images of nanosized HIAM-4017 (a) and HIAM-4018 (d); selectivity test of nanosized HIAM-4017 (b) and HIAM-4018 (e) in aqueous solution toward different anions (anion concentration = 10  $\mu\text{M}$ ); concentration-dependent emission quenching of nanosized HIAM-4017 with  $\text{Cr}_2\text{O}_7^{2-}$  concentrations of 2, 4, 6, 8, 20, 40, and 80  $\mu\text{M}$  (c) and HIAM-4018 with  $\text{Cr}_2\text{O}_7^{2-}$  concentrations of 2, 6, 8, 10, 20, 40, and 60  $\mu\text{M}$  (f) and the corresponding Stern–Volmer plot.

nature and phase purity. This result also reveals that the introduction of the OH group has no effect on the formation of the Olympic rings-inspired structure. HIAM-4018 also exhibits high thermal stability and remains crystalline up to 500  $^{\circ}\text{C}$  as confirmed by TGA and temperature-dependent in situ PXRD analysis (Figures S14 and S15). The optical absorption and emission spectra of HIAM-4018 measured at room temperature show maxima at 378 and 533 nm, respectively, with the corresponding PLQY of 24.2% under 365 nm excitation (Figure 4d). A Stokes shift of 155 nm was recorded for HIAM-4018, which is only 64 nm for HIAM-4017. The large Stokes shift can be attributed to the emission from the keto form of BIHTA confined into HIAM-4018 matrix after excitation, which demonstrates a highly efficient ESIPT process. Notably, as shown in Figure 4d, the spectral overlap between the emission and absorption spectra of HIAM-4018 is very small, suggesting that such an ESIPT material with the large Stokes shift can significantly reduce self-absorption. Similar to HIAM-4017, the emission behavior of HIAM-4018 shows little change after being treated in pH = 4 and pH = 10 aqueous solutions for 24 h (Figure S16).

To gain a deeper understanding of the ESIPT in HIAM-4018, we investigated the excitation and emission process of  $\text{H}_4\text{BIHTA}$  using time-dependent density functional theory (TD-DFT). The geometries of the ground-state ( $S_0$ ) and first singlet excited-state ( $S_1$ ) local minima were optimized with the CAM-B3LYP/cc-pVDZ method and the electronic energies were refined with the CAM-B3LYP/cc-pVTZ method. The N–H distance in the geometries of the enol form species  $\text{E-S}_0$  and  $\text{E-S}_1$  are 1.67 and 1.50  $\text{\AA}$  and the O–H bond lengths are 1.00 and 1.05  $\text{\AA}$ , respectively (Figure 4e). It suggests that the  $S_1$  relaxation of  $\text{E-S}_0$  favors the reduction of the N–H distance and elongation of the O–H bond length. The keto form in the  $S_1$  minimum ( $\text{K-S}_1$ ) shows a N–H bond of 1.03  $\text{\AA}$  and a O–H

distance of 1.85  $\text{\AA}$ . However, the geometry optimization of  $\text{K-S}_0$  directly leads to  $\text{E-S}_0$ , suggesting a strong preference of the ground-state reverse proton transfer. The  $S_1$  excitation of  $\text{E-S}_0$  corresponds to a  $\pi\pi^*$  transition of one electron from the highest occupied molecular orbital (HOMO) to the lowest unoccupied molecular orbital (LUMO). The electronic transition depicts the excited-state charge transfer from the benzimidazole and phenol moieties to the terminal phenyl rings (Figure S17). The  $\text{E-S}_1$  shows a similar nature of electronic transitions. However, the HOMO of  $\text{K-S}_1$  is mainly localized at the benzoquinone moiety instead of delocalizing over the benzimidazole ring (Figure S17). The computed  $S_1$  excitation energy of  $\text{E-S}_0$  is 3.93 eV (315 nm) (Figure 4f), which agrees with the experimental absorption wavelength ( $\sim 378$  nm, Figure 4d). The predicted  $S_1$  emission energy of  $\text{E-S}_1$  is 3.45 eV (360 nm) with a Stokes shift of 45 nm. In contrast, the emission energy of  $\text{K-S}_1$  is 2.73 eV (455 nm). It agrees with the experimental emission wavelength ( $\sim 533$  nm) and leads to a notable Stokes shift of 140 nm, in line with the experimental result (155 nm, Figure 4d). The energy profile in Figure 4f shows that  $\text{K-S}_1$  (3.41 eV) is 0.36 eV lower than  $\text{E-S}_1$  (3.77 eV), which explains the energetic driving force of the ESIPT in HIAM-4018. The experimental results as well as the calculated data support the efficient ESIPT in HIAM-4018.

**Nanosized MOFs for Sensing.** Because of the excellent chemical and thermal stability and strong emission of HIAM-4017 and HIAM-4018, we looked further into their possible applications as chemical sensors. As it is essential to achieve high dispersibility of the sensor materials for aqueous phase-based sensing and imaging,<sup>48–51</sup> we prepared both MOFs in nanosized crystals via a mixed-acid strategy (see synthesis details in the Supporting Information). As shown in Figure 5a, d, HIAM-4017 and HIAM-4018 with a size of about 300 nm were obtained. PXRD patterns clearly indicate the phase purity



of the as-synthesized nanosized HIAM-4017 and HIAM-4018 (Figure S18).

Various anions ( $F^-$ ,  $Cl^-$ ,  $Br^-$ ,  $I^-$ ,  $CO_3^{2-}$ ,  $HCO_3^-$ ,  $CH_3COO^-$ ,  $IO_4^-$ ,  $SO_3^{2-}$ ,  $SO_4^{2-}$ ,  $NO_2^-$ , and  $Cr_2O_7^{2-}$ ) were then added to the aqueous suspension of nanosized HIAM-4017 and HIAM-4018 to explore their sensing ability to common anions. Remarkably, only  $Cr_2O_7^{2-}$  exhibited significant emission quenching with quenching percentages of 40.4 and 58.4% in 10  $\mu M$   $Cr_2O_7^{2-}$ , respectively (Figure Sb, e). Both HIAM-4017 and HIAM-4018 exhibit fast response time for the detection of  $Cr_2O_7^{2-}$ , reaching about 70% quenching maximum within seconds and saturation in 3 min (Figure S19). These results are comparable with the good-performing MOFs.<sup>39,52–54</sup> Other common anions resulted in a much less fluorescence quenching effect. These results indicate that both MOFs, especially HIAM-4018, can be utilized as a highly selective chemical sensor for the detection of  $Cr_2O_7^{2-}$  in the aqueous phase. The titration experiments were carried out to determine the sensitivity of HIAM-4017 and HIAM-4018 for  $Cr_2O_7^{2-}$  detection. As shown in Figure 5c, f, the emission intensities gradually decrease for both HIAM-4017 and HIAM-4018 with increasing  $Cr_2O_7^{2-}$  concentration. Based on the Stern–Volmer equation, a linear correlation coefficient of 0.998 was obtained for HIAM-4017 in the  $Cr_2O_7^{2-}$  concentration range from 2 to 80  $\mu M$ , while for HIAM-4018, the value is 0.993 in the range from 2 to 60  $\mu M$ . Accordingly, the detection limits for  $Cr_2O_7^{2-}$  were calculated to be 0.6 and 0.05  $\mu M$  for HIAM-4017 and HIAM-4018, respectively, which is comparable with several previously reported MOFs.<sup>39,52</sup> These results demonstrate that HIAM-4017 and HIAM-4018 exhibit excellent sensitivity and selectivity for  $Cr_2O_7^{2-}$  detection.

The PXRD patterns of HIAM-4017 and HIAM-4018 after  $Cr_2O_7^{2-}$  titration are almost identical to those before sensing (Figure S18), which further confirms the chemical stability of these MOFs. As reported,<sup>39</sup> the mechanism for  $Cr_2O_7^{2-}$ -induced emission quenching can be attributed, at least partially, to the energy transfer from the MOF to  $Cr_2O_7^{2-}$  because of the appreciable spectral overlap between the absorption spectrum of  $Cr_2O_7^{2-}$  (Figure S20) and the emission spectra of HIAM-4017 and HIAM-4018. Compared to HIAM-4017, the lower detection limit of HIAM-4018 might be attributed to the fact that the synergistic effect of  $Cr_2O_7^{2-}$ -caused energy transfer and blocked ESIPT.

## CONCLUSIONS

In conclusion, we have demonstrated the successful construction of a unique MOF, (4,8)-c HIAM-4017, structurally inspired by the Olympic rings and guided by reticular chemistry. The structure of HIAM-4017 represents an unprecedented underlying net topology termed jcs. It is obtained by the judicious design and synthesis of a nonsymmetric organic linker and its incorporation in the Zr-based framework. In addition, ESIPT functionality was introduced via linker functionalization to its isoreticular MOF, HIAM-4018, inducing a large Stokes shift of 155 nm. Nanosized HIAM-4017 and HIAM-4018 exhibit excellent performance for  $Cr_2O_7^{2-}$  detection with high sensitivity and selectivity. The successful implementation of reticular chemistry in synthesizing Olympic rings-inspired MOFs with the ESIPT property opens a new avenue for the advancement in achieving next-generation porous materials with the target-specific structure and properties.

## ASSOCIATED CONTENT

### Supporting Information

The Supporting Information is available free of charge at <https://pubs.acs.org/doi/10.1021/jacs.2c09832>.

Materials; organic linker and MOF synthesis; single-crystal structure; and other additional information (PDF)

### Accession Codes

CCDC 2204363 contains the supplementary crystallographic data for this paper. These data can be obtained free of charge via [www.ccdc.cam.ac.uk/data\\_request/cif](http://www.ccdc.cam.ac.uk/data_request/cif), or by emailing [data\\_request@ccdc.cam.ac.uk](mailto:data_request@ccdc.cam.ac.uk), or by contacting The Cambridge Crystallographic Data Centre, 12 Union Road, Cambridge CB2 1EZ, UK; fax: +44 1223 336033.

## AUTHOR INFORMATION

### Corresponding Authors

Lu-Lu Qu – School of Chemistry and Materials Science, Jiangsu Normal University, Xuzhou 221116, P.R. China; [orcid.org/0000-0001-5458-3457](https://orcid.org/0000-0001-5458-3457); Email: [luluqu@jnu.edu.cn](mailto:luluqu@jnu.edu.cn)

Xiao-Yuan Liu – Hoffmann Institute of Advanced Materials, Shenzhen Polytechnic, Shenzhen 518055, P.R. China; [orcid.org/0000-0003-2400-8085](https://orcid.org/0000-0003-2400-8085); Email: [liuxiaoyuan1989@szpt.edu.cn](mailto:liuxiaoyuan1989@szpt.edu.cn)

Jing Li – Hoffmann Institute of Advanced Materials, Shenzhen Polytechnic, Shenzhen 518055, P.R. China; Department of Chemistry and Chemical Biology, Rutgers University, Piscataway, New Jersey 08854, United States; [orcid.org/0000-0001-7792-4322](https://orcid.org/0000-0001-7792-4322); Email: [jingli@rutgers.edu](mailto:jingli@rutgers.edu)

### Authors

Jincheng Si – School of Chemistry and Materials Science, Jiangsu Normal University, Xuzhou 221116, P.R. China; Hoffmann Institute of Advanced Materials, Shenzhen Polytechnic, Shenzhen 518055, P.R. China

Hai-Lun Xia – Hoffmann Institute of Advanced Materials, Shenzhen Polytechnic, Shenzhen 518055, P.R. China

Kang Zhou – Hoffmann Institute of Advanced Materials, Shenzhen Polytechnic, Shenzhen 518055, P.R. China

Jingbai Li – Hoffmann Institute of Advanced Materials, Shenzhen Polytechnic, Shenzhen 518055, P.R. China

Kai Xing – Department of Chemistry, College of Basic Medicine, Third Military Medical University (Army Medical University), Chongqing 400038, P.R. China

Jiafeng Miao – Hoffmann Institute of Advanced Materials, Shenzhen Polytechnic, Shenzhen 518055, P.R. China

Jian Zhang – Hoffmann Institute of Advanced Materials, Shenzhen Polytechnic, Shenzhen 518055, P.R. China

Hao Wang – Hoffmann Institute of Advanced Materials, Shenzhen Polytechnic, Shenzhen 518055, P.R. China; [orcid.org/0000-0001-7732-778X](https://orcid.org/0000-0001-7732-778X)

Complete contact information is available at:

<https://pubs.acs.org/10.1021/jacs.2c09832>

### Author Contributions

The manuscript was written through contributions of all authors. J.S. and H.-L.X. contributed equally to this work.

### Funding

National Natural Science Foundation of China (No. 22201185, 21974055), Shenzhen Science and Technology Program (No. RCBS20200714114941230), Jiangsu Province

Key Research and Development Program (Social Development) (No. BE2022707), and the Xuzhou Science and Technology Key R&D Program (Social Development) Project (No. KC20178).

## Notes

The authors declare no competing financial interest.

## ACKNOWLEDGMENTS

The authors gratefully acknowledge the support from Shenzhen Polytechnic, the National Natural Science Foundation of China (No. 22201185, 21974055), the Shenzhen Science and Technology Program (No. RCBS20200714114941230), the Jiangsu Province Key Research and Development Program (Social Development) (No. BE2022707), and the Xuzhou Science and Technology Key R&D Program (Social Development) Project (No. KC20178).

## REFERENCES

- (1) Furukawa, H.; Cordova, K. E.; O'Keeffe, M.; Yaghi, O. M. The Chemistry and Applications of Metal–Organic Frameworks. *Science* **2013**, *341*, No. 1230444.
- (2) Adil, K.; Belmabkhout, Y.; Pillai, R. S.; Cadiau, A.; Bhatt, P. M.; Assen, A. H.; Maurin, G.; Eddaoudi, M. Gas/vapour separation using ultra-microporous metal–organic frameworks: insights into the structure/separation relationship. *Chem. Soc. Rev.* **2017**, *46*, 3402–3430.
- (3) Trickett, C. A.; Helal, A.; Al-Maythaly, B. A.; Yamani, Z. H.; Cordova, K. E.; Yaghi, O. M. The chemistry of metal–organic frameworks for CO<sub>2</sub> capture, regeneration and conversion. *Nat. Rev. Mater.* **2017**, *2*, 17045.
- (4) Jiao, L.; Wang, Y.; Jiang, H. L.; Xu, Q. Metal–Organic Frameworks as Platforms for Catalytic Applications. *Adv. Mater.* **2018**, *30*, No. e1703663.
- (5) Bavykina, A.; Kolobov, N.; Khan, I. S.; Bau, J. A.; Ramirez, A.; Gascon, J. Metal–Organic Frameworks in Heterogeneous Catalysis: Recent Progress, New Trends, and Future Perspectives. *Chem. Rev.* **2020**, *120*, 8468–8535.
- (6) Islamoglu, T.; Chen, Z.; Wasson, M. C.; Buru, C. T.; Kirlikovali, K. O.; Afrin, U.; Mian, M. R.; Farha, O. K. Metal–Organic Frameworks against Toxic Chemicals. *Chem. Rev.* **2020**, *120*, 8130–8160.
- (7) Lustig, W. P.; Mukherjee, S.; Rudd, N. D.; Desai, A. V.; Li, J.; Ghosh, S. K. Metal–organic frameworks: functional luminescent and photonic materials for sensing applications. *Chem. Soc. Rev.* **2017**, *46*, 3242–3285.
- (8) Wang, H.; Lustig, W. P.; Li, J. Sensing and capture of toxic and hazardous gases and vapors by metal–organic frameworks. *Chem. Soc. Rev.* **2018**, *47*, 4729–4756.
- (9) Zhao, Y.; Zeng, H.; Zhu, X.-W.; Lu, W.; Li, D. Metal–organic frameworks as photoluminescent biosensing platforms: mechanisms and applications. *Chem. Soc. Rev.* **2021**, *50*, 4484–4513.
- (10) Yaghi, O. M. Reticular Chemistry—Construction, Properties, and Precision Reactions of Frameworks. *J. Am. Chem. Soc.* **2016**, *138*, 15507–15509.
- (11) Yaghi, O. M.; O'Keeffe, M.; Ockwig, N. W.; Chae, H. K.; Eddaoudi, M.; Kim, J. Reticular synthesis and the design of new materials. *Nature* **2003**, *423*, 705–714.
- (12) Ockwig, N. W.; Delgado-Friedrichs, O.; O'Keeffe, M.; Yaghi, O. M. Reticular Chemistry: Occurrence and Taxonomy of Nets and Grammar for the Design of Frameworks. *Acc. Chem. Res.* **2005**, *38*, 176–182.
- (13) Yaghi, O. M.; Kalmutzki, M. J.; Diercks, C. S. *Introduction to Reticular Chemistry*; Wiley, 2019; pp. 1–494.
- (14) O'Keeffe, M.; Peskov, M. A.; Ramsden, S. J.; Yaghi, O. M. The Reticular Chemistry Structure Resource (RCSR) Database of, and Symbols for Crystal Nets. *Acc. Chem. Res.* **2008**, *41*, 1782–1789.
- (15) Chen, Z.; Hanna, S. L.; Redfern, L. R.; Alezi, D.; Islamoglu, T.; Farha, O. K. Reticular chemistry in the rational synthesis of functional zirconium cluster-based MOFs. *Coord. Chem. Rev.* **2019**, *386*, 32–49.
- (16) Liu, Y.; O'Keeffe, M.; Treacy, M. M. J.; Yaghi, O. M. The geometry of periodic knots, polycatenanes and weaving from a chemical perspective: a library for reticular chemistry. *Chem. Soc. Rev.* **2018**, *47*, 4642–4664.
- (17) Chen, Z.; Jiang, H.; Li, M.; O'Keeffe, M.; Eddaoudi, M. Reticular Chemistry 3.2: Typical Minimal Edge-Transitive Derived and Related Nets for the Design and Synthesis of Metal–Organic Frameworks. *Chem. Rev.* **2020**, *120*, 8039–8065.
- (18) Feng, L.; Wang, K.-Y.; Lv, X.-L.; Yan, T.-H.; Li, J.-R.; Zhou, H.-C. Modular Total Synthesis in Reticular Chemistry. *J. Am. Chem. Soc.* **2020**, *142*, 3069–3076.
- (19) Freund, R.; Canossa, S.; Cohen, S. M.; Yan, W.; Deng, H.; Guillerm, V.; Eddaoudi, M.; Madden, D. G.; Fairen-Jimenez, D.; Lyu, H.; Macreadie, L. K.; Ji, Z.; Zhang, Y.; Wang, B.; Haase, F.; Wöll, C.; Zaremba, O.; Andreo, J.; Wuttke, S.; Diercks, C. S. 25 Years of Reticular Chemistry. *Angew. Chem., Int. Ed.* **2021**, *60*, 23946–23974.
- (20) Catarineu, N. R.; Schoedel, A.; Urban, P.; Morla, M. B.; Trickett, C. A.; Yaghi, O. M. Two Principles of Reticular Chemistry Uncovered in a Metal–Organic Framework of Heterotritropic Linkers and Infinite Secondary Building Units. *J. Am. Chem. Soc.* **2016**, *138*, 10826–10829.
- (21) Chen, Z.; Weseliński, Ł. J.; Adil, K.; Belmabkhout, Y.; Shkurenko, A.; Jiang, H.; Bhatt, P. M.; Guillerm, V.; Dauzon, E.; Xue, D.-X.; O'Keeffe, M.; Eddaoudi, M. Applying the Power of Reticular Chemistry to Finding the Missing alb-MOF Platform Based on the (6,12)-Coordinated Edge-Transitive Net. *J. Am. Chem. Soc.* **2017**, *139*, 3265–3274.
- (22) Guillerm, V.; Grancha, T.; Imaz, I.; Juanhuix, J.; Maspoch, D. Zigzag Ligands for Transversal Design in Reticular Chemistry: Unveiling New Structural Opportunities for Metal–Organic Frameworks. *J. Am. Chem. Soc.* **2018**, *140*, 10153–10157.
- (23) Chen, Z.; Thiam, Z.; Shkurenko, A.; Weseliński, Ł. J.; Adil, K.; Jiang, H.; Alezi, D.; Assen, A. H.; O'Keeffe, M.; Eddaoudi, M. Enriching the Reticular Chemistry Repertoire with Minimal Edge-Transitive Related Nets: Access to Highly Coordinated Metal–Organic Frameworks Based on Double Six-Membered Rings as Net-Coded Building Units. *J. Am. Chem. Soc.* **2019**, *141*, 20480–20489.
- (24) Zhang, Y.-F.; Zhang, Z.-H.; Ritter, L.; Fang, H.; Wang, Q.; Space, B.; Zhang, Y.-B.; Xue, D.-X.; Bai, J. New Reticular Chemistry of the Rod Secondary Building Unit: Synthesis, Structure, and Natural Gas Storage of a Series of Three-Way Rod Amide-Functionalized Metal–Organic Frameworks. *J. Am. Chem. Soc.* **2021**, *143*, 12202–12211.
- (25) Chen, Z.; Li, P.; Zhang, X.; Li, P.; Wasson, M. C.; Islamoglu, T.; Stoddart, J. F.; Farha, O. K. Reticular Access to Highly Porous aco-MOFs with Rigid Trigonal Prismatic Linkers for Water Sorption. *J. Am. Chem. Soc.* **2019**, *141*, 2900–2905.
- (26) Diercks, C. S.; Liu, Y.; Cordova, K. E.; Yaghi, O. M. The role of reticular chemistry in the design of CO<sub>2</sub> reduction catalysts. *Nat. Mater.* **2018**, *17*, 301–307.
- (27) Chen, Z.; Li, P.; Anderson, R.; Wang, X.; Zhang, X.; Robison, L.; Redfern, L. R.; Moribe, S.; Islamoglu, T.; Gómez-Gualdrón, D. A.; Yildirim, T.; Stoddart, J. F.; Farha, O. K. Balancing volumetric and gravimetric uptake in highly porous materials for clean energy. *Science* **2020**, *368*, 297–303.
- (28) He, T.; Kong, X.-J.; Zhou, J.; Zhao, C.; Wang, K.; Wu, X.-Q.; Lv, X.-L.; Si, G.-R.; Li, J.-R.; Nie, Z.-R. A Practice of Reticular Chemistry: Construction of a Robust Mesoporous Palladium Metal–Organic Framework via Metal Metathesis. *J. Am. Chem. Soc.* **2021**, *143*, 9901–9911.
- (29) Guillerm, V.; Maspoch, D. Geometry Mismatch and Reticular Chemistry: Strategies To Assemble Metal–Organic Frameworks with Non-default Topologies. *J. Am. Chem. Soc.* **2019**, *141*, 16517–16538.
- (30) Jiang, H.; Alezi, D.; Eddaoudi, M. A reticular chemistry guide for the design of periodic solids. *Nat. Rev. Mater.* **2021**, *6*, 466–487.

- (31) Kalmutzki, M. J.; Hanikel, N.; Yaghi, O. M. Secondary building units as the turning point in the development of the reticular chemistry of MOFs. *Sci. Adv.* **2018**, *4*, No. eaat9180.
- (32) Chen, Z.; Kirlikovali, K. O.; Li, P.; Farha, O. K. Reticular Chemistry for Highly Porous Metal–Organic Frameworks: The Chemistry and Applications. *Acc. Chem. Res.* **2022**, *55*, 579–591.
- (33) Amabilino, D. B.; Ashton, P. R.; Reder, A. S.; Spencer, N.; Stoddart, J. F. Olympiadane. *Angew. Chem., Int. Ed.* **1994**, *33*, 1286–1290.
- (34) Lu, C.-H.; Qi, X.-J.; Cecconello, A.; Jester, S.-S.; Famulok, M.; Willner, I. Switchable Reconfiguration of an Interlocked DNA Olympiadane Nanostructure. *Angew. Chem., Int. Ed.* **2014**, *53*, 7499–7503.
- (35) Datta, S.; Kato, Y.; Higashiharaguchi, S.; Aratsu, K.; Isobe, A.; Saito, T.; Prabhu, D. D.; Kitamoto, Y.; Hollamby, M. J.; Smith, A. J.; Dalglish, R.; Mahmoudi, N.; Pesce, L.; Perego, C.; Pavan, G. M.; Yagai, S. Self-assembled poly-catenanes from supramolecular toroidal building blocks. *Nature* **2020**, *583*, 400–405.
- (36) Feng, D.; Gu, Z.-Y.; Li, J.-R.; Jiang, H.-L.; Wei, Z.; Zhou, H.-C. Zirconium-Metalloporphyrin PCN-222: Mesoporous Metal–Organic Frameworks with Ultrahigh Stability as Biomimetic Catalysts. *Angew. Chem., Int. Ed.* **2012**, *51*, 10307–10310.
- (37) Mondloch, J. E.; Bury, W.; Fairen-Jimenez, D.; Kwon, S.; DeMarco, E. J.; Weston, M. H.; Sarjeant, A. A.; Nguyen, S. T.; Stair, P. C.; Snurr, R. Q.; Farha, O. K.; Hupp, J. T. Vapor-Phase Metalation by Atomic Layer Deposition in a Metal–Organic Framework. *J. Am. Chem. Soc.* **2013**, *135*, 10294–10297.
- (38) Wang, B.; Wang, P.; Xie, L.-H.; Lin, R.-B.; Lv, J.; Li, J.-R.; Chen, B. A stable zirconium based metal-organic framework for specific recognition of representative polychlorinated dibenzo-p-dioxin molecules. *Nat. Commun.* **2019**, *10*, 3861.
- (39) He, T.; Zhang, Y.-Z.; Kong, X.-J.; Yu, J.; Lv, X.-L.; Wu, Y.; Guo, Z.-J.; Li, J.-R. Zr(IV)-Based Metal-Organic Framework with T-Shaped Ligand: Unique Structure, High Stability, Selective Detection, and Rapid Adsorption of  $\text{Cr}_2\text{O}_7^{2-}$  in Water. *ACS Appl. Mater. Interfaces* **2018**, *10*, 16650–16659.
- (40) Ghasempour, H.; Wang, K.-Y.; Powell, J. A.; ZareKarizi, F.; Lv, X.-L.; Morsali, A.; Zhou, H.-C. Metal–organic frameworks based on multicarboxylate linkers. *Coord. Chem. Rev.* **2021**, *426*, No. 213542.
- (41) Padalkar, V. S.; Seki, S. Excited-state intramolecular proton-transfer (ESIPT)-inspired solid state emitters. *Chem. Soc. Rev.* **2016**, *45*, 169–202.
- (42) Jayaramulu, K.; Kanoo, P.; George, S. J.; Maji, T. K. Tunable emission from a porous metal–organic framework by employing an excited-state intramolecular proton transfer responsive ligand. *Chem. Commun.* **2010**, *46*, 7906–7908.
- (43) Chen, L.; Ye, J.-W.; Wang, H.-P.; Pan, M.; Yin, S.-Y.; Wei, Z.-W.; Zhang, L.-Y.; Wu, K.; Fan, Y.-N.; Su, C.-Y. Ultrafast water sensing and thermal imaging by a metal-organic framework with switchable luminescence. *Nat. Commun.* **2017**, *8*, 15985.
- (44) Li, Y.-P.; Zhu, X.-H.; Li, S.-N.; Jiang, Y.-C.; Hu, M.-C.; Zhai, Q.-G. Highly Selective and Sensitive Turn-Off–On Fluorescent Probes for Sensing  $\text{Al}^{3+}$  Ions Designed by Regulating the Excited-State Intramolecular Proton Transfer Process in Metal–Organic Frameworks. *ACS Appl. Mater. Interfaces* **2019**, *11*, 11338–11348.
- (45) Huang, P.; Liu, Y.; Karmakar, A.; Yang, Q.; Li, J.; Wu, F.-Y.; Deng, K.-Y. Tuning the excited-state intramolecular proton transfer (ESIPT)-based luminescence of metal–organic frameworks by metal nodes toward versatile photoluminescent applications. *Dalton Trans.* **2021**, *50*, 6901–6912.
- (46) Ghosh, A.; Sikdar, N.; Maji, T. K. An excited-state intramolecular proton-transfer responsive nanoscale MOF for dual sensing of water and chromate ions. *J. Mater. Chem. C* **2022**, *10*, 7558–7566.
- (47) Trannoy, V.; Guillou, N.; Livage, C.; Roch-Marchal, C.; Haouas, M.; Léaustic, A.; Allain, C.; Clavier, G.; Yu, P.; Devic, T. Fluorescent Zr(IV) Metal–Organic Frameworks Based on an Excited-State Intramolecular Proton Transfer-Type Ligand. *Inorg. Chem.* **2019**, *58*, 6918–6926.
- (48) Park, J.; Jiang, Q.; Feng, D.; Mao, L.; Zhou, H. C. Size-Controlled Synthesis of Porphyrinic Metal–Organic Framework and Functionalization for Targeted Photodynamic Therapy. *J. Am. Chem. Soc.* **2016**, *138*, 3518–3525.
- (49) Wang, S.; McGuirk, C. M.; d’Aquino, A.; Mason, J. A.; Mirkin, C. A. Metal–Organic Framework Nanoparticles. *Adv. Mater.* **2018**, *30*, No. e1800202.
- (50) Marshall, C. R.; Staudhammer, S. A.; Brozek, C. K. Size control over metal–organic framework porous nanocrystals. *Chem. Sci.* **2019**, *10*, 9396–9408.
- (51) Cai, X.; Xie, Z.; Li, D.; Kassymova, M.; Zang, S.-Q.; Jiang, H.-L. Nano-sized metal-organic frameworks: Synthesis and applications. *Coord. Chem. Rev.* **2020**, *417*, No. 213366.
- (52) Lv, R.; Wang, J.; Zhang, Y.; Li, H.; Yang, L.; Liao, S.; Gu, W.; Liu, X. An amino-decorated dual-functional metal–organic framework for highly selective sensing of Cr(III) and Cr(VI) ions and detection of nitroaromatic explosives. *J. Mater. Chem. A* **2016**, *4*, 15494–15500.
- (53) Lin, Z.-J.; Zheng, H.-Q.; Zheng, H.-Y.; Lin, L.-P.; Xin, Q.; Cao, R. Efficient Capture and Effective Sensing of  $\text{Cr}_2\text{O}_7^{2-}$  from Water Using a Zirconium Metal–Organic Framework. *Inorg. Chem.* **2017**, *56*, 14178–14188.
- (54) Wang, X.; Zhang, Y.; Shi, Z.; Lu, T.; Wang, Q.; Li, B. Multifunctional Zr-MOF Based on Bisimidazole Tetracarboxylic Acid for pH Sensing and Photoreduction of Cr(VI). *ACS Appl. Mater. Interfaces* **2021**, *13*, 54217–54226.

## Recommended by ACS

### Building a shp: A Rare-Earth Metal–Organic Framework and Its Application in a Catalytic Photooxidation Reaction

Victor Quezada-Novoa, Ashlee J. Howarth, *et al.*

MAY 27, 2021  
CHEMISTRY OF MATERIALS

READ 

### Tuning Metal–Organic Framework (MOF) Topology by Regulating Ligand and Secondary Building Unit (SBU) Geometry: Structures Built on 8-Connected $\text{M}_6$ ( $\text{M} = \text{Zr}, \dots$ )

Xingyu Li, Jing Li, *et al.*

NOVEMBER 01, 2022  
JOURNAL OF THE AMERICAN CHEMICAL SOCIETY

READ 

### Construction of Highly Proton-Conductive Zr(IV)-Based Metal–Organic Frameworks From Pyrrolo-pyrrole-Based Linkers with a Rhombic Shape

Yiyang Li, Wei Huang, *et al.*

JULY 26, 2021  
INORGANIC CHEMISTRY

READ 

### Two Robust Isorecticular Metal–Organic Frameworks with Different Interpenetration Degrees Exhibiting Disparate Breathing Behaviors

Yueying Zhu, Yunling Liu, *et al.*

JULY 06, 2022  
INORGANIC CHEMISTRY

READ 

Get More Suggestions >